Journal of Alloys and Compounds 959 (2023) 170571

Contents lists available at ScienceDirect

Journal of Alloys and Compounds

journal homepage: www.elsevier.com/locate/jalcom

Flash synthesis of ultrafine and active NiRu alloy nanoparticles on N-rich carbon nanotubes via joule heating for efficient hydrogen and oxygen evolution reaction

Jin Li [a,1], Chengbin Wang [a,1], Xiaoyu Chen [b], Yu Zhang [a], Yuanyuan Zhang [a], Kaicai Fan [c], Lingbo Zong [a,*], Lei Wang [a]

[a] Key Laboratory of Eco-chemical Engineering, College of Chemistry and Molecular Engineering, Qingdao University of Science and Technology, Qingdao 266042, China
[b] College of Materials Science and Engineering, Shenzhen University, Shenzhen 518060, China
[c] College of Materials Science and Engineering, Qingdao University of Science and Technology, Qingdao 266042, China

ARTICLE INFO

Article history:
Received 16 March 2023
Received in revised form 29 April 2023
Accepted 13 May 2023
Available online 15 May 2023

Keywords:
Joule heating
Alloy nanoparticles
Hydrogen evolution reaction (HER)
Oxygen evolution reaction (OER)
Strong metal-support interaction

ABSTRACT

The design and controlled synthesis of high-performance alloy nanoparticles as bifunctional electrocatalysts towards hydrogen evolution reaction (HER) and oxygen evolution reaction (OER) is of great industrial importance, but remains a great challenge. However, most of the prepared bimetallic alloys display unsatisfactory catalytic activity. Herein, NiRu alloy nanoparticles well-dispersed on N-rich carbon nanotubes (NiRu-CNTs) with a strong metal-support interaction (SMSI) are prepared through a flash Joule heating method in 0.5 s. Impressively, NiRu-CNTs exhibit remarkable HER activity under 1.0 M KOH solution with quite a small overpotential of 5.1 mV to reach the current density of 10 mA cm^{-2}. In addition, superior HER stability up to 10 h with no noticeable current density degradation is realized. As expected, NiRu-CNTs exhibits excellent OER performance with a small overpotential of 270 mV at 10 mA cm^{-2}, small Tafel slope of 54.1 mV dec^{-1}, and long-term durability over 5000 CV cycles. When used in two-electrode electrolyzer for overall water splitting, NiRu-CNTs displays a low voltage of 1.85 V at 100 mA cm^{-2}. This eco-friendly and cost-effective synthesis approach can be extended to the rational synthesis of various alloy catalysts with different metal species.

1. Introduction

Electrochemical water splitting including cathodic hydrogen evolution reaction (HER), and anodic oxygen evolution reaction (OER), which can obtain sustainable hydrogen and oxygen from water, is considered as a very promising method to reach zero carbon emission [1–4]. However, both HER and OER require high overpotentials to overcome the large kinetic barriers [5–7]. Consequently, active electrocatalysts are needed to reduce the reaction energy barrier, improve the reaction kinetics and achieve high catalytic efficiency. Currently, Pt and RuO_2 benchmarks are considered to be the optimal electrocatalysts for HER and OER, respectively, but their expensive nature and scarcity remain major challenges for the large-scale applications [8,9]. Therefore, it is imperative to minimize the usage of those noble metals when developing highly active bifunctional HER and OER electrocatalysts.

Ru, as a member of platinum group metals, has attracted great attention with excellent activity and superior stability in electrochemical N_2 reduction reaction, oxygen reduction reaction, and coupling of amines and alcohols [10–14]. Ru-based materials are virtually promising candidates for HER and OER [15–18]. Considering the high cost and scarcity, the wide application of Ru is hampered. Fortunately, alloying Ru with earth abundant 3d-transition metals is an effective strategy to reduce the usage of Ru and improve the HER and OER activity [19–21]. For example, RuCu nanotubes were prepared for water splitting, which can reduce the free energy of adsorption hydrogen (ΔG_H^*) and largely decrease the free energy change (for rate-determining step) of OER [22]. In addition, Liu et al. synthesized RuNi nanosheets with optimized water dissociation capacity and good HER performance [23]. Despite those progress, the methods of preparing alloys mainly focus on the time-consuming

* Corresponding author.
E-mail address: lingbozong@qust.edu.cn (L. Zong).
[1] These authors contributed equally.

https://doi.org/10.1016/j.jallcom.2023.170571
0925-8388/

high temperature pyrolysis and solvothermal reactions. Therefore, the development of Ru-based catalysts via ultrafast, facile and low-cost strategy is still a significant issue.

Carbon-based materials with good electron transfer capacity and corrosion resistance are ideal supports for metal nanoparticles. The strong metal-support interaction (SMSI) can not only prevent the agglomeration of nanoparticles but also effectively boost the anchoring ability for nanoparticles [24]. This suggests that SMSI can greatly promote the activity and stability of the catalysts [25–27]. Thus, anchoring Ru-based alloys stably on carbon support is highly desired to achieve superior HER, OER, and overall water splitting activity. Joule heating strategy, which possesses flash heating and cooling process, has been reported as a facile method to load nanoparticles on carbon support. During the flash heating process, the ultrahigh temperature can actuate the "fission" and "fusion" of metal precursors, which lead to the homogeneous mixing of elements. Afterwards, the flash cooling rate can promote the production of crystalline nanoparticles [28,29]. Hence, Joule heating technique with flash ramp rates can effectively regulate the particle size, crystalline structure and dispersibility [30,31]. Notably, Ni-based materials have become promising electrocatalysts due to their abundant earth reserves, low cost, and similar electronic properties to Pt [32–34]. In these regards, exploring facile Joule heating strategy to alloy Ni with Ru, which are expected to achieve fine electronic of catalysts [21,35,36], on carbon supports are fascinating to construct efficient bifunctional electrocatalysts.

Herein, we developed an eco-friendly, cost-effective and ultrafast synthesis method for the construction of ultrafine and active NiRu alloy nanoparticles, which are well-dispersed on N-rich carbon nanotubes (NiRu-CNTs) by Joule heating strategy in 0.5 s. Specifically, this flash heating and cooling process induces the explosive nucleation and restricts the grain growth, resulting in the uniform distribution of ultrafine NiRu alloy nanoparticles on N-rich carbon nanotubes [37,38]. As expected, NiRu-CNTs displays superior catalytic activities and cycling stabilities. For HER in 1.0 M KOH, NiRu-CNTs show drastically small overpotential of 5.1 mV at the current density of 10 mA cm^{-2}, low Tafel slopes of 31.3 mV dec^{-1}, and stable cycling stability even after 5000 cycles. Specifically, NiRu-CNTs exhibits remarkable activity at the large current density of 100 mA cm^{-2}, and it needs an overpotential of only 42.6 mV. In addition, NiRu-CNTs can attain satisfying OER performance with low overpotential of 270 mV at 10 mA cm^{-2}, small Tafel slope of 54.1 mV dec^{-1}. NiRu-CNTs exhibit superior OER stability without obvious voltage increase at the large current density of 100 mA cm^{-2} for least 5000 cycles. Importantly, the optimized two-electrode electrolyzer with NiRu-CNTs displays low cell voltages of 1.59 V at 10 mA cm^{-2} in 1.0 M KOH solution, much lower than Pt/C + RuO_2. The two-electrode water-splitting device also displays superior stability up to 12 h.

2. Experimental section

2.1. Chemicals

$NiCl_2{\cdot}6\ H_2O$ (Sinopharm, analytical purity), $NH_3{\cdot}H_2O$ (Sinopharm, 28%), cetyltrimethylammonium bromide (CTAB, Aladdin, ≥98%), $RuCl_3$ (Aladdin, 45%–55%) were used to synthesize the required catalysts.

2.2. Synthesis of $[Ni(NH_4)_6]Cl_2$

The $NiCl_2{\cdot}6\ H_2O$ was dissolved in 10 mL deionized water, and then, the solution was slowly added to 40 mL concentrated ammonia in ice water, and stirred in an ice water bath for 15 min. The obtained precipitate was dried in air after extraction and washed with ethanol. After drying, purple crystals of $[Ni(NH_4)_6]Cl_2$ were obtained.

2.3. Synthesis of NiRu-CNTs

The CNTs were firstly modified using 0.8 mM CTAB solution. Specifically, 29 mg of CTAB was dispersed in 100 mL of deionized water, and CTAB was fully dissolved by multiple sonication treatment. Then, 50 mg of CNTs were dispersed in 50 mL of CTAB solution by continuous ultrasonication for 3 h and stirring for 24 h. After centrifugation and drying, 30 mg CTAB decorated CNTs (CNTs@CTAB) were sufficiently ground with 30 mg $RuCl_3$ and 7.5 mg $[Ni(NH_4)_6]Cl_2$. Finally, the mixture was pyrolyzed under the protection of N_2 atmosphere at 1200 °C via Joule heating in 0.5 s. The obtained product was named as NiRu-CNTs.

2.4. Synthesis of Ni-CNTs and Ru-CNTs

In order to investigate the alloying effect, reference samples of Ni-CNTs and Ru-CNTs were prepared using the same synthetic method as NiRu-CNTs without the addition of $RuCl_3$ and $[Ni(NH_4)_6]Cl_2$, respectively.

2.5. Characterization

The crystalline phase structures of the synthesized materials were studied by X-ray diffraction (XRD, Cu Kα, λ = 1.5406 Å) in the 2θ range of 5°– 85° at a scan rate of 5° min^{-1}. Raman spectroscopy analysis (inVia, Spectral range: 800–4000 wave number) was used to characterize the defects of the as-developed electrocatalysts. Scanning electron microscope (SEM, regulus 8100) and transmission electron microscope (TEM, JEM-2100PLUS) were used to investigate the morphology. X-ray photoelectron spectroscopy (XPS, Thermo Scientific ESCALAB 250Xi) was used to verify the elemental composition and oxidation state. The contents of Ru and Ni in NiRu-CNTs were tested by inductively coupled plasma mass spectrometry (ICP-MS, Agilent 730).

2.6. Electrochemical testing

Electrochemical measurements including linear sweep voltammetry (LSV) and cyclic voltammetry (CV) were performed using an electrochemical workstation (CHI 760E) with a three-electrode configuration. Rotating disk electrode (RDE) coated by the electrocatalysts were used as working electrode. Carbon rods and Hg/HgO electrode were used as counter and reference electrodes, respectively. CV was performed at a sweep rate of 100 mV s^{-1} before electrochemical testing. LSV tests were performed at a sweep rate of 5 mV s^{-1} in 1.0 M KOH. All electrochemical impedance spectroscopy (EIS) tests were performed on electrochemical workstation (Gamry, Interface 5000E). Stability tests were done by conducting chronoamperometry and accelerated cycle testing, respectively. For overall water splitting test, 1 cm^2 carbon paper with the electrocatalyst loading capacity of 0.25 mg cm^{-2} were used as the working electrodes. All the electrolytes used were freshly prepared 1.0 M KOH solution.

The double-layer capacitance (C_{dl}) was obtained by testing the CV in the range of 0.674–0.774 V. Electrochemical active surface area (ECSA) was calculated using the following equation [39]:

$$ECSA = C_{dl}/C_s$$

where C_s is 40 μF cm^{-2}.

Here is the formula for Faradaic efficiency:

$$Faradaic\quad efficiency = (nF \times m)/Q$$

where n = 4 for OER (2 for HER), F = 96485.3 C mol^{-1}, m = the moles number of O_2 (H_2), Q = It.

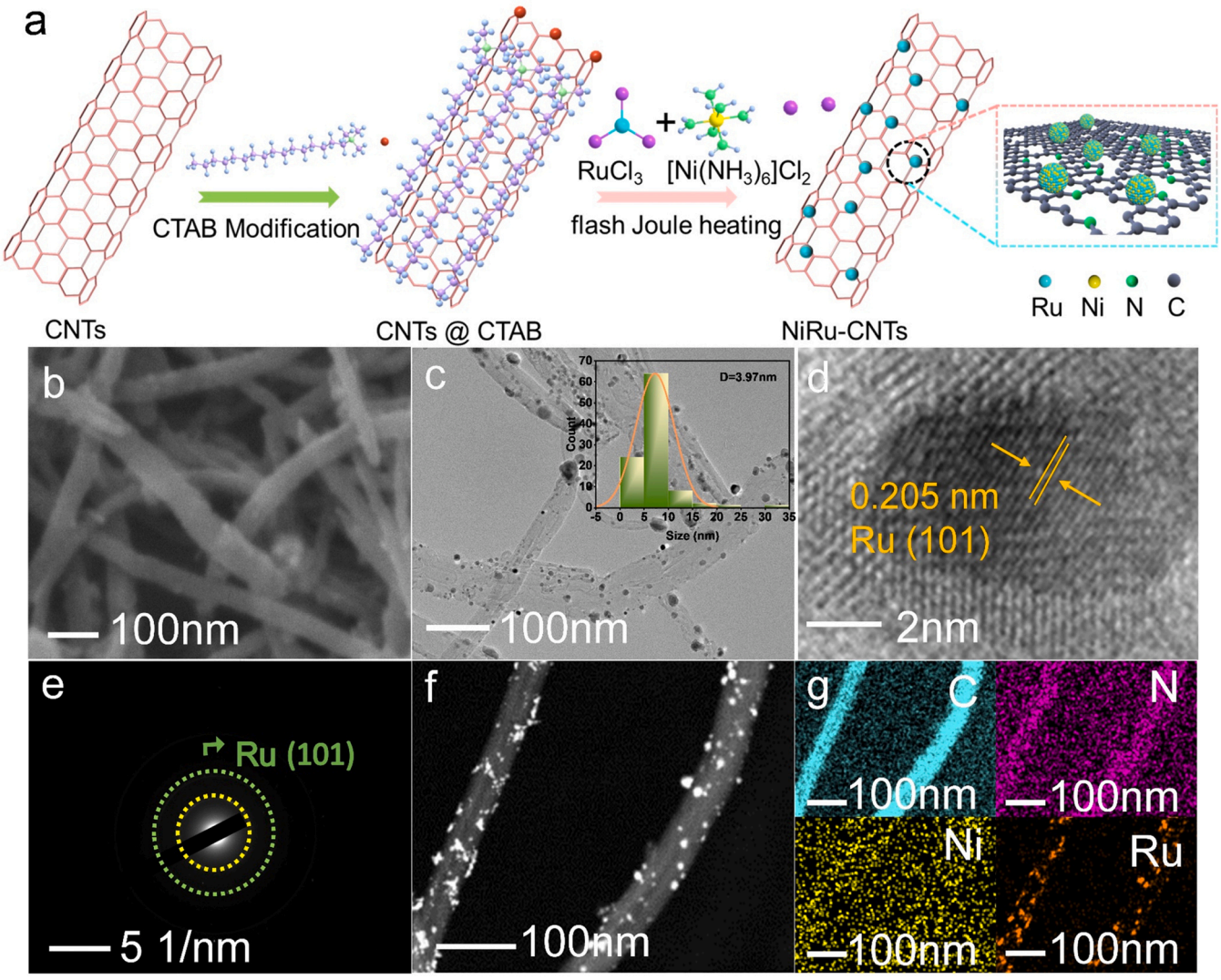

Fig. 1. Synthesis and characterizations of NiRu-CNTs. (a) Schematic diagram of NiRu-CNTs catalyst. (b) SEM, (c) TEM (Inset: Particle size distribution of nanoparticles), (d) HR-TEM, and (e) SAED images of NiRu-CNTs. (f) HAADF image and (g) EDX elemental mapping images of NiRu-CNTs.

For the electrochemical test in 0.5 M H_2SO_4 and 1.0 M PBS, same three-electrode configuration as the test in 1.0 M KOH was used except that Ag/AgCl electrode was applied as reference electrodes.

The potentials in this work were given with respect to the reversible hydrogen electrode (RHE). All directly obtained potentials versus Hg/HgO were converted to versus RHE according to the following equation:

$$E_{RHE} = E_{Hg/HgO} + 0.059pH + 0.098 - 0.95iR$$

The obtained potentials versus Ag/AgCl were converted to versus RHE according to the following equation:

$$E_{RHE} = E_{Ag/AgCl} + 0.059pH + 0.1976 - 0.95iR$$

3. Results and discussions

3.1. Synthesis and characterizations of NiRu-CNTs

NiRu-CNTs was synthesized via the Joule heating strategy in 0.5 s as illustrated in Fig. 1a. CTAB, which is an ionic surfactant, is widely used as a guiding agent to synthesize metal nanoparticles with unique structures for efficient electrocatalysts [40]. Thus, CTAB decorated CNTs (CNTs@CTAB) were used as carbon support for metal nanoparticles. Meanwhile, transition metal complexes $[Ni(NH_3)_6]Cl_2$ with good stability under harsh conditions was chosen as Ni source [41,42]. Subsequently, CNTs@CTAB, $RuCl_3$ and $[Ni(NH_3)_6]Cl_2$ were placed in a mortar and ground thoroughly to ensure the uniform dispersion of metal species. Finally, NiRu-CNTs was obtained by calcination of above mixtures at 1200 °C for 0.5 ss via Joule heating method. The morphology of NiRu-CNTs was investigated by SEM and TEM. SEM images in Fig. 1b and Fig. S1 display that NiRu-CNTs a similar tubular morphology as initial CNTs, indicating that Joule heating cannot damage the morphology and structure of CNTs. TEM image in Fig. 1c exhibits that ultrafine alloy nanoparticles with a uniform particle size of 5–10 nm in diameter are well dispersed onto the CNTs. The detected D-spacings for NiRu-CNTs in Fig. 1d is 0.205 nm, which is in agreement with the plane (101) of hexagonal close packing (hcp) Ru [43]. The similar result is testified by selected area electron diffraction (SAED) in Fig. 1e. In the high-angle annular dark-field scanning TEM (HAADF-STEM) image (Fig. 1f), the bright ultrafine nanoparticles are identified. As depicted in Fig. 1g, the energy dispersive X-ray spectroscopy (EDX) elemental mapping images confirm the coexistence of Ni and Ru elements, and Ni and Ru share a similar distribution in NiRu-CNTs. Interestingly, the uniform dispersion of N element across the CNTs indicates that CNTs is an N-rich conductive carrier, which contributes significantly to the

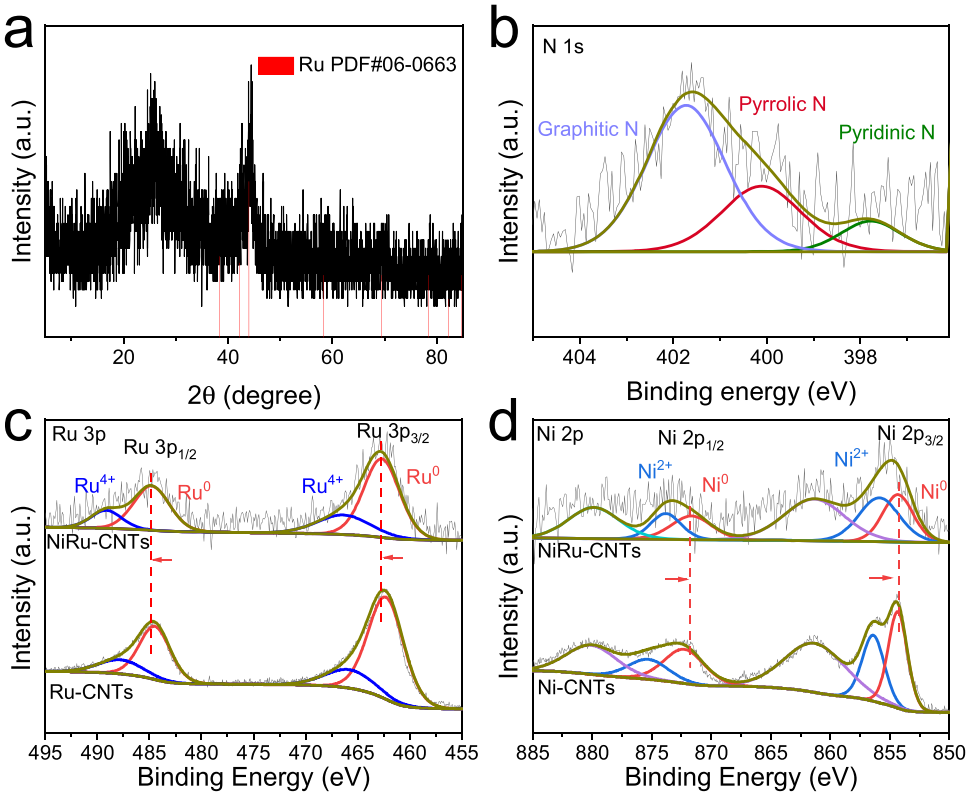

Fig. 2. XRD and XPS study of NiRu-CNTs. (a) XRD pattern of NiRu-CNTs. High-resolution XPS of (b) N 1 s of NiRu-CNTs, (c) Ru 3p of NiRu-CNTs and Ru-CNTs, (d) Ni 2p of NiRu-CNTs and Ni-CNTs.

improvement of catalytic property. The actual loading of Ni and Ru for NiRu-CNTs are 2.99 wt% and 15.32 wt%, respectively, detected by the inductively coupled plasma mass spectrometry (ICP-MS). Thus, the atomic ratio between Ni and Ru in NiRu alloys is 1:3. To explore the alloying effect, Ru-CNTs (Fig. S2) and Ni-CNTs (Fig. S3) are synthesized as references, which display the similar morphology structure with NiRu-CNTs.

Fig. 2a shows the crystalline phase of NiRu-CNTs characterized by XRD. The diffraction peak located at around 23° can be assigned to (002) crystal plane of CNTs, and the diffraction peaks appearing at 38.38°, 42.11°, 43.97° are attributed to hcp structure of metal alloys as hcp Ru (PDF: #06–0663) [44]. Notably, there is no other diffraction peak can be observed, identifying the successful fabrication of NiRu alloys, which is in good agreement with the above TEM and HAADF-STEM results. Raman spectrum of NiRu-CNTs shows two peaks of G-peak at 1450 cm^{-1} and D-peak at 1350 cm^{-1} (Fig. S4). The low I_D/I_G intensity ratio of 0.61 suggests the high graphitization degree and electrical conductivity [45].

The X-ray photoelectron spectroscopy (XPS) was used to study the electronic property of NiRu-CNTs. The XPS survey spectrum confirms the presence of C, N, Ni, and Ru elements on the surface of NiRu-CNTs (Fig. S5). As shown in Fig. 2b, the high-resolution N 1 s displays three peaks at 401.7 eV, 400.1 eV and 397.8 eV, which can be attributed to graphitic N, pyrrolic N and pyridinic N, respectively [46,47]. The existent pyridinic N may be favorable to the improvement of HER and OER process [48]. For the high-resolution Ru 3p XPS spectrum (Fig. 2c), the binding energy of Ru 3p in NiRu-CNTs showed a positive shift after the introduction of Ni element, testifying that the charge transfer between Ni and Ru. Fig. 2d presents the high-resolution Ni 2p XPS spectra, which suggests the existence of Ni metallic and Ni^{2+}. The remaining peaks are attributed to the satellite peaks [35]. Apparently, the peaks of Ni 2p XPS spectrum in NiRu-CNTs shifts slightly towards lower binding energies compared to those in Ni-CNTs, suggesting efficient electronic coupling effect between Ru and Ni [49]. The electronic coupling effect is expected to alter the electronic state of metal alloys and optimize the adsorption free energy of intermediates for catalytic reaction [35].

3.2. Evaluation of the electrochemical properties for HER

The electrochemical evaluation for HER of NiRu-CNTs was evaluated by a three-electrodes configuration in 1.0 M KOH saturated with N_2. The linear sweep voltammetry (LSV) polarization curves of NiRu-CNTs are shown in Fig. 3a, where 20 wt% Pt/C, Ni-CNTs and Ru-CNTs are used as reference samples. The overpotentials at the current density of 10 mA cm^{-2} and 100 mA cm^{-2} are crucial indicators for HER electrocatalysts. As revealed by Fig. 3b, Ni-CNTs and Ru-CNTs display poor HER activity with large overpotentials of 329.3 mV and 89.8 mV at 10 mA cm^{-2}, and Ru-CNTs exhibits an overpotential as large as 249.1 mV at 100 mA cm^{-2}. It is worth noting that the required overpotentials for NiRu-CNTs to attain 10 mA cm^{-2} and 100 mA cm^{-2} are only 5.1 mV and 42.6 mV, respectively. Obviously, these overpotentials are significantly lower than Pt/C (31.6 mV, and 118.7 mV) and previously reported electrocatalysts (Table S1), and this demonstrates that alloying is an important mean to boost catalytic properties. In addition, excellent HER performance of NiRu-CNTs in a wide-range of pH is expected. As shown in Fig. S6, NiRu-CNTs catalysts display extremely low overpotential of 120.3 mV and 57.9 mV under the current density of 10 mA cm^{-2} towards HER in 0.5 M H_2SO_4 and 1.0 M PBS, respectively.

In 1.0 M KOH solution, NiRu-CNTs displays a small Tafel slope of only 31.3 mV dec^{-1}, which is much lower than that of Pt/C (46.3 mV dec^{-1}), Ni-CNTs (164.5 mV dec^{-1}) and Ru-CNTs (104.6 mV dec^{-1}), indicating that NiRu-CNTs has fastest reaction kinetics and the Tafel step is the rate-determining step in the whole HER process [50]. Electrochemically active surface area (ECSA) is also an important aspect to evaluate the catalytic performance of HER. Therefore, we estimated the ECSA of NiRu-CNTs and reference samples based on

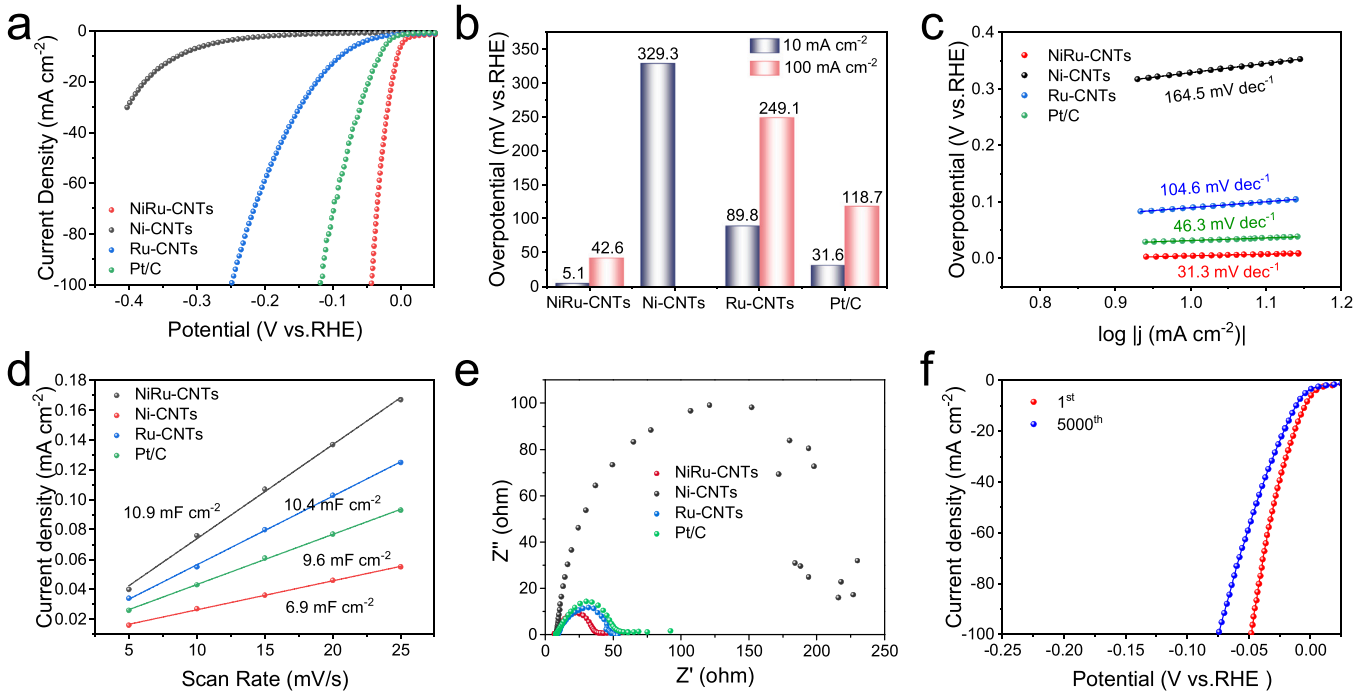

Fig. 3. Electrocatalytic HER performance in 1.0 M KOH. (a) LSV curves of HER for NiRu-CNTs, Ni-CNTs, Ru-CNTs, and Pt/C. (b) Comparison of the overpotentials of NiRu-CNTs, Ni-CNTs, Ru-CNTs, and Pt/C at 10 mA cm^{-2} and 100 mA cm^{-2}, respectively. (c) Corresponding Tafel plots of NiRu-CNTs, Ni-CNTs, Ru-CNTs, and Pt/C. (d) Fitting curves of double-layer capacitance (C_{dl}) of NiRu-CNTs, Ni-CNTs, Ru-CNTs, and Pt/C. (e) Nyquist plots of NiRu-CNTs, Ni-CNTs, Ru-CNTs, and Pt/C. (f) Polarization curves of NiRu-CNTs were recorded before and after 5000 CV cycles test.

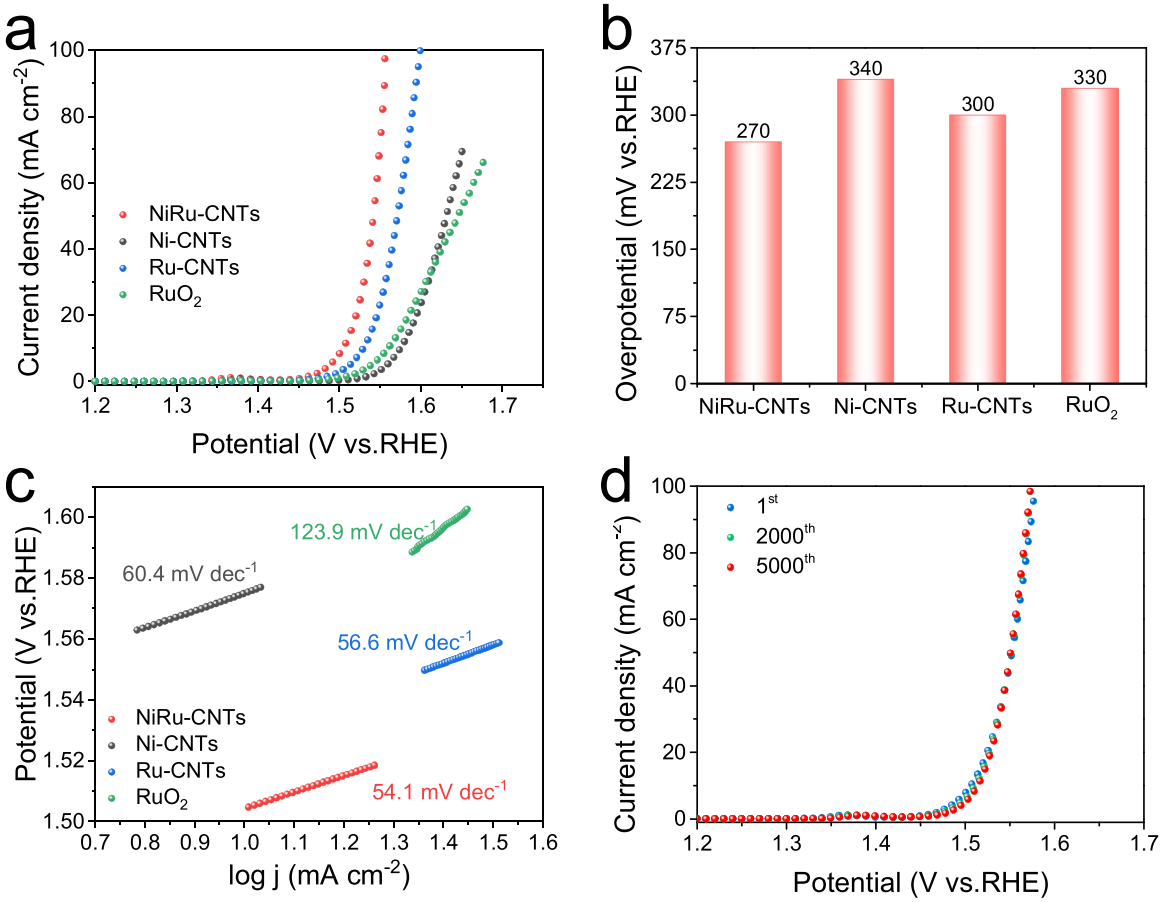

Fig. 4. Electrochemical OER performance of NiRu-CNTs and benchmark RuO_2 in O_2-saturated 1.0 M KOH solution. (a) OER LSV curves of NiRu-CNTs and control samples. (b) The overpotentials comparison of NiRu-CNTs and control samples at 10 mA cm^{-2}. (c) Corresponding Tafel slopes of NiRu-CNTs, Ni-CNTs, Ru-CNTs and RuO_2. (d) OER polarization curves of NiRu-CNTs before and after 2000 and 5000 cycles.

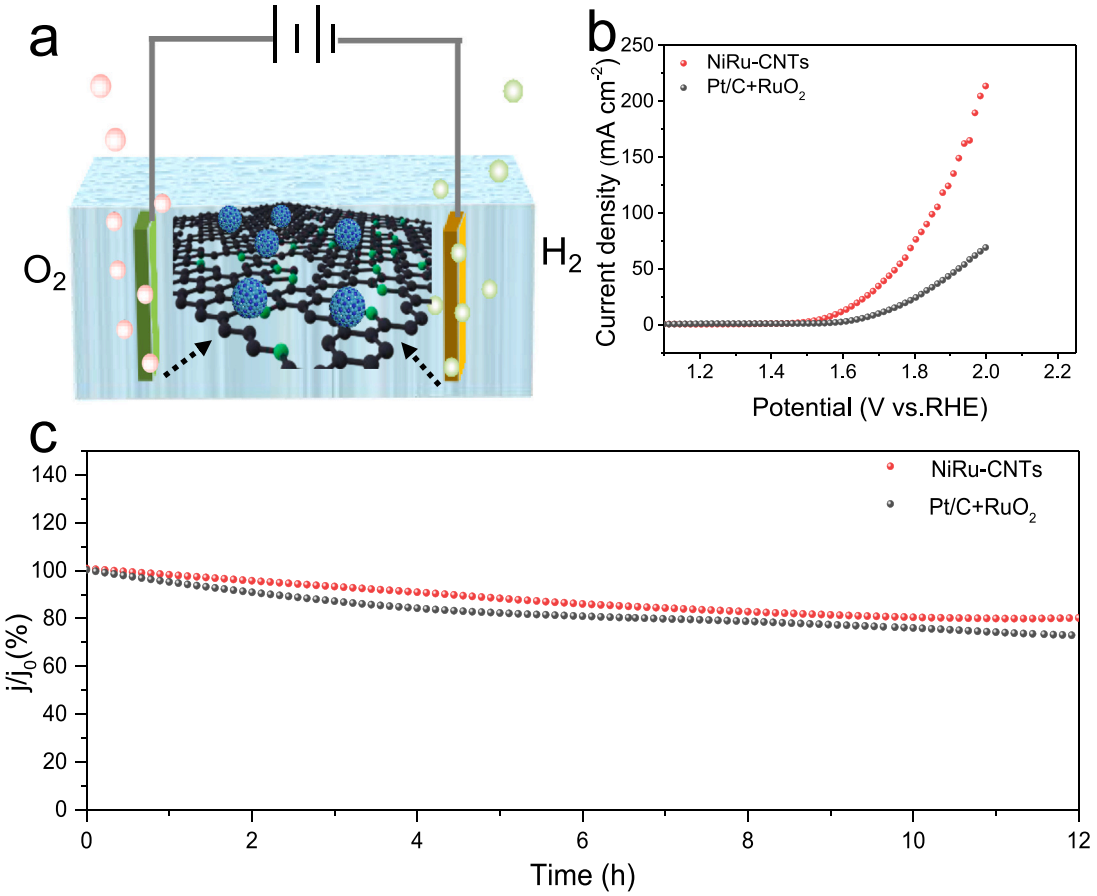

Fig. 5. The overall water splitting performance of NiRu-CNTs and Pt/C+RuO_2 in 1.0 M KOH solution. (a) Diagram of the device for overall water splitting. (b) Polarization curves of two-electrode electrolyzer using NiRu-CNTs and Pt/C+RuO_2. (c) Chronoamperometric test of NiRu-CNTs and control sample at 1.60 V.

the double-layer capacity (C_{dl}) method [51,52]. Fig. S7 shows the CV curves of NiRu-CNTs, Pt/C, Ni-CNTs and Ru-CNTs at different sweep rates in the potential window from 0.674 V (vs. RHE) to 0.774 V (vs. RHE), respectively. As can be seen in Fig. 3d, the value of obtained C_{dl} for NiRu-CNTs is 10.9 mF cm^{-2}, much higher than Pt/C (9.6 mF cm^{-2}), Ni-CNTs (6.9 mF cm^{-2}) and Ru-CNTs (10.4 mF cm^{-2}). The ECSA of NiRu-CNTs is determined to be 272.5 cm^2 (Fig. S8), which is much larger than Pt/C (240 cm^2), Ni-CNTs (172.5 cm^2) and Ru-CNTs (260 cm^2). The largest ECSA of NiRu-CNTs suggests the more exposed active sites, which may be ascribed to small-size alloy effects. In addition, electrochemical impedance spectroscopy (EIS) was used to further explore the charge transfer rates of electrochemical hydrogen generation (Fig. 3e). The charge-transfer resistance (R_{ct}) value for NiRu-CNTs is 29.5 Ω, which is much smaller than Pt/C (48.5 Ω), Ni-CNTs (254.8 Ω) and Ru-CNTs (40.2 Ω). The EIS results confirm that NiRu-CNTs has the fastest charge transfer capacity at the electrode/electrolyte interface. This is attributed to the high graphitization degree of NiRu-CNTs, which is consistent with the previous Raman test result.

Accelerated cycling measurements were performed to evaluate the durability of NiRu-CNTs, as shown in Fig. 3 f, where the potential decay of only 7 mV is observed after 5000 CV cycles. In addition, chronoamperometry as counterparts was conducted, as shown in Fig. S9, the current density of NiRu-CNTs maintains almost constant for 10 h, while Pt/C undergoes a substantial decrease. All the above results testify that the as-developed NiRu-CNTs via Joule heating method has remarkable long-term stability. The encouraging HER activity and durability may be induced by the following effects: The strong SMSI between NiRu alloy nanoparticles and N-rich CNTs can prevent the falling off of alloy nanoparticles and boost the stability of as-developed NiRu-CNTs. The rich active sites of NiRu-CNTs with excellent electrolyte penetration and mass transport are beneficial for the superior HER catalytic performance.

3.3. Evaluation of the electrochemical properties for OER

The electrocatalytic OER performance of NiRu-CNTs was then evaluated in 1.0 M KOH. Ni-CNTs, Ru-CNTs and RuO_2 were chosen as control samples. The results of OER LSV curves are shown in Fig. 4a. At 10 mA cm^{-2}, NiRu-CNTs presents the smallest overpotential of only 270 mV in comparison with that of Ni-CNTs (340 mV), Ru-CNTs (300 mV) and RuO_2 (330 mV), revealing the excellent OER activity of NiRu-CNTs (Fig. 4b). Furthermore, the OER overpotential of NiRu-CNTs required to reach 10 mA cm^{-2} are 271 mV and 460 mV in 0.5 M H_2SO_4 and 1.0 M PBS solution, respectively, while the overpotential of RuO_2 under the corresponding conditions are 272 mV and 750 mV, respectively (Fig. S10). Meanwhile, NiRu-CNTs has a low Tafel slope (54.1 mV dec^{-1}), which is much lower than RuO_2 (123.9 mV dec^{-1}), Ni-CNTs (60.4 mV dec^{-1}) and Ru-CNTs (56.6 mV dec^{-1}), indicating that the prepared NiRu-CNTs has fast O_2 generation kinetics (Fig. 4c). To evaluate the stability of NiRu-CNTs, accelerated cycling test with a sweep rate of 100 mV s^{-1} was conducted. After 2000 and 5000 CV cycling testing, negligible shift of potential is observed (Fig. 4d). We further investigated the stability by chronoamperometry method at a constant potential of 1.50 V (Fig. S11). It is worth noting that the current density of NiRu-CNTs has almost no attenuation after 11 h durability test, which highlights the excellent stability of NiRu-CNTs. Moreover, NiRu-CNTs displays no obvious change inn morphology structure after this

long-term OER testing, confirming that NiRu-CNTs has excellent structural stability (Fig. S12).

3.4. Electrochemical assessment for overall water splitting

Benefit from the excellent HER and OER activity and stability of NiRu-CNTs, the overall water splitting performance was examined in a typical two-electrode electrolyzer in 1.0 M KOH solution (Fig. 5a and Fig. S13). The cell voltage at the current density of 10 mA cm^{-2} is usually considered as indicator to check out the quality of as-developed electrocatalyst. The electrocatalytic measurement for overall water splitting was conducted at a scan rate of 5 mV s^{-1}. As depicted in Fig. 5b, the cell voltage of NiRu-CNTs is 1.59 V at 10 mA cm^{-2}, which is 110 mV lower than that of Pt/C+RuO_2. To be highlighted, the cell potential of NiRu-CNTs is 1.74 V at 50 mA cm^{-2}, which is 180 mV lower than Pt/C+RuO_2, further confirming the ultrahigh intrinsic activity of as-constructed NiRu-CNTs. Further, the chronoamperometric records show that NiRu-CNTs has a minor attenuation of only 20% after 12 h test under a constant potential of 1.60 V, while it is 27% for Pt/C+RuO_2 (Fig. 5c). Notably, NiRu-CNTs delivers greatly enhanced stability. Moreover, the morphology structure of NiRu-CNTs remains practically the same before long-term stability test (Fig. S14).

To investigate the energy-conversion efficiency of electrocatalytic reaction on NiRu-CNTs, we calculated the Faradaic efficiency of NiRu-CNTs for overall water splitting at a constant current density of 50 mA cm^{-2} and a constant voltage of 1.75 V, respectively (Fig. S15, Fig. S16, Fig. S17 and Fig. S18). By comparing the experimental amount of H_2 and O_2 measured by the drainage method with the theoretically calculated values, we found that the amounts of evolved gases agree well with the theoretically calculated values and the yield of H_2 is nearly twice as much as O_2. Therefore, the Faradaic efficiency of NiRu-CNTs obtained by both methods is close to 100%, and no obvious side reactions occurred during HER and OER processes. This result further demonstrates that the as-developed NiRu-CNTs are auspicious electrocatalysts for efficient and economical water-splitting device.

4. Conclusion

In conclusion, we successfully synthesized ultrafine and active NiRu alloy nanoparticles well-dispersed on N-rich CNTs via an eco-friendly and cost-effective flash Joule heating strategy. Owing to the alloying of Ni and Ru, the strong SMSI between alloy nanoparticles and N-rich CNTs, and efficient charge/mass transfer, robust HER and OER catalytic performances for NiRu-CNTs are observed. In 1.0 M KOH solution, the as-developed NiRu-CNTs displays ultralow HER overpotentials of 5.1 mV and 42.6 mV at 10 mA cm^{-2} and 100 mA cm^{-2}, respectively. It also demonstrates an ultralow Tafel slope of 31.3 mV dec^{-1}, and outstanding robustness with negligible activity loss. In addition, the rather low OER overpotential, good stability, and fast O_2 release kinetics are also observed for NiRu-CNTs in 1.0 M KOH. NiRu-CNTs can be directly employed as bifunctional electrocatalyst for two-electrode electrolyzer with superior robustness and 100% Faradaic yield. This work strongly demonstrates that Joule heating is an important strategy for the preparation of well-dispersed alloys with ultrasmall dimension and a wide range of applications.

CRediT authorship contribution statement

Jin Li: Investigation, Visualization, Data curation. **Chengbin Wang:** Visualization, Data curation. **Xiaoyu Chen:** Visualization. **Yu Zhang:** Investigation, Data curation. **Yuanyuan Zhang:** Data curation. **Kaicai Fan:** Data curation. **Lingbo Zong:** Conceptualization, Investigation, Visualization, Formal analysis, Writing – review & editing, Funding acquisition. **Lei Wang**: Investigation.

Data Availability

Data will be made available on request.

Declaration of Competing Interest

The authors declare that they have no known competing financial interests or personal relationships that could have appeared to influence the work reported in this paper.

Acknowledgements

This work was supported financially by the National Natural Science Foundation of China, China (Grant No. 52172208), China Postdoctoral Science Foundation (Grant No. 2022M712167).

Appendix A. Supporting information

Supplementary data associated with this article can be found in the online version at doi:10.1016/j.jallcom.2023.170571.

References

[1] M. Qu, Y. Jiang, M. Yang, S. Liu, Q. Guo, W. Shen, M. Li, R. He, Regulating electron density of NiFe-P nanosheets electrocatalysts by a trifle of Ru for high-efficient overall water splitting, Appl. Catal. B: Environ. 263 (2020) 118324.
[2] Y. Zhang, S. Chen, Y. Zhang, R. Li, B. Zhao, T. Peng, Hydrogen-bond regulation of microenvironment of Ni (II)-porphyrin bifunctional electrocatalysts for efficient overall water splitting, Adv. Mater. (2023), https://doi.org/10.1002/adma.202210727
[3] S. Liu, Y. Jiang, M. Yang, M. Zhang, Q. Guo, W. Shen, R. He, M. Li, Highly conductive and metallic cobalt-nickel selenide nanorods supported on Ni foam as an efficient electrocatalyst for alkaline water splitting, Nanoscale 11 (2019) 7959–7966.
[4] J. Gu, Y. Peng, T. Zhou, J. Ma, H. Pang, Y. Yamauchi, Porphyrin-based framework materials for energy conversion, Nano Res. Energy 1 (2022) 9120009.
[5] L. Li, P. Wang, Q. Shao, X. Huang, Recent progress in advanced electrocatalyst design for acidic oxygen evolution reaction, Adv. Mater. 33 (2021) 2004243.
[6] F. Gao, J. He, H. Wang, J. Lin, R. Chen, K. Yi, F. Huang, Z. Lin, M. Wang, Te-mediated electro-driven oxygen evolution reaction, Nano Res. Energy 1 (2022) 9120029.
[7] W. Zhang, L. Cui, J. Liu, Recent advances in cobalt-based electrocatalysts for hydrogen and oxygen evolution reactions, J. Alloy. Compd. 821 (2020) 153542.
[8] G. Zhan, Y. Yao, F. Quan, H. Gu, X. Liu, L. Zhang, D-band frontier: a new hydrogen evolution reaction activity descriptor of Pt single-atom catalysts, J. Energy Chem. 72 (2022) 203.
[9] D. Escalera-López, S. Czioska, J. Geppert, A. Boubnov, P. Röse, E. Saraci, U. Krewer, J.-D. Grunwaldt, S. Cherevko, Phase-and surface composition-dependent electrochemical stability of Ir-Ru nanoparticles during oxygen evolution reaction, ACS Catal. 11 (2021) 9300.
[10] Z. Geng, Y. Liu, X. Kong, P. Li, K. Li, Z. Liu, J. Du, M. Shu, R. Si, J. Zeng, Achieving a record-high yield rate of 120.9 for N_2 electrochemical reduction over Ru single-atom catalysts, Adv. Mater. 30 (2018) 1803498.
[11] T. Wu, M.M. Melander, K. Honkala, Coadsorption of NRR and HER intermediates determines the performance of Ru-N_4 toward electrocatalytic N_2 reduction, ACS Catal. 12 (2022) 2505.
[12] L. Cui, K. Fan, L. Zong, F. Lu, M. Zhou, B. Li, L. Zhang, L. Feng, X. Li, Y. Chen, Sol-gel pore-sealing strategy imparts tailored electronic structure to the atomically dispersed Ru sites for efficient oxygen reduction reaction, Energy Storage Mater. 44 (2022) 469.
[13] V. Cherepakhin, T.J. Williams, Catalyst evolution in ruthenium-catalyzed coupling of amines and alcohols, ACS Catal. 10 (2019) 56.
[14] P. Mukherjee, I.M. Patil, M. Lokanathan, H. Parse, B. Kakade, A. Swami, Ru decorated Pt_2CoNi/C nanoparticles as a proficient electrocatalyst for oxygen reduction reaction, J. Alloy. Compd. 918 (2022) 165520.
[15] X. Cao, J. Huo, L. Li, J. Qu, Y. Zhao, W. Chen, C. Liu, H. Liu, G. Wang, Recent advances in engineered Ru-based electrocatalysts for the hydrogen/oxygen conversion reactions, Adv. Energy Mater. 12 (2022) 2202119.
[16] M. You, X. Du, X. Hou, Z. Wang, Y. Zhou, H. Ji, L. Zhang, Z. Zhang, S. Yi, D. Chen, In-situ growth of ruthenium-based nanostructure on carbon cloth for superior electrocatalytic activity towards HER and OER, Appl. Catal. B: Environ. 317 (2022) 121729.
[17] P. Li, W. Wei, J. Li, Y. Liu, K. Fan, L. Zong, L. Wang, Flash Joule heating synthesis of carbon supported ultrafine metallic heterostructures for high-performance overall water splitting, J. Alloy. Compd. 947 (2023) 169630.

[18] L. Shang, J.-Q. Wang, C.-Q. Cheng, Y. Zhang, F.-F. Zhang, Y.-M. Xie, J.-D. Lu, J. Mao, Q.-J. Guo, C.-K. Dong, Oxidized single nickel atoms embedded in Ru matrix for highly efficient hydrogen evolution reaction, J. Alloy. Compd. 874 (2021) 159909.
[19] W. Wei, P. Li, F. Lu, K. Fan, B. Li, Y. Wei, L. Zong, L. Wang, Loading uniformly distributed CuRu alloys on carbon nanotubes via flash Joule heating for high-performance electrocatalytic water splitting, J. Alloy. Compd. 936 (2023) 168349.
[20] H. Huang, H. Jung, C.-Y. Park, S. Kim, A. Lee, H. Jun, J. Choi, J.W. Han, J. Lee, Surface conversion derived core-shell nanostructures of Co particles@RuCo alloy for superior hydrogen evolution in alkali and seawater, Appl. Catal. B: Environ. 315 (2022) 121554.
[21] Q. Yang, P. Jin, B. Liu, L. Zhao, J. Cai, Z. Wei, S. Zuo, J. Zhang, L. Feng, Ultrafine carbon encapsulated NiRu alloys as bifunctional electrocatalysts for boosting overall water splitting: morphological and electronic modulation through minor Ru alloying, J. Mater. Chem. A 8 (2020) 9049.
[22] D. Cao, X. Huang, H. Zhang, W. Liu, D. Cheng, Constructing porous RuCu nanotubes with highly efficient alloy phase for water splitting in different pH conditions, Chem. Eng. J. 456 (2023) 141148.
[23] G. Liu, W. Zhou, B. Chen, Q. Zhang, X. Cui, B. Li, Z. Lai, Y. Chen, Z. Zhang, L. Gu, Synthesis of RuNi alloy nanostructures composed of multilayered nanosheets for highly efficient electrocatalytic hydrogen evolution, Nano Energy 66 (2019) 104173.
[24] W. Karim, C. Spreafico, A. Kleibert, J. Gobrecht, J. VandeVondele, Y. Ekinci, J.A. van Bokhoven, Catalyst support effects on hydrogen spillover, Nature 541 (2017) 68.
[25] H. Chen, Z. Yang, X. Wang, F. Polo-Garzon, P.W. Halstenberg, T. Wang, X. Suo, S.-Z. Yang, H.M. Meyer III, Z. Wu, Photoinduced strong metal-support interaction for enhanced catalysis, J. Am. Chem. Soc. 143 (2021) 8521.
[26] X. Wu, Z. Wang, D. Zhang, Y. Qin, M. Wang, Y. Han, T. Zhan, B. Yang, S. Li, J. Lai, Solvent-free microwave synthesis of ultra-small Ru-Mo_2C@CNT with strong metal-support interaction for industrial hydrogen evolution, Nat. Commun. 12 (2021) 4018.
[27] W. Yu, H. Huang, Y. Qin, D. Zhang, Y. Zhang, K. Liu, Y. Zhang, J. Lai, L. Wang, The synergistic effect of pyrrolic-N and pyridinic-N with Pt under strong metal-support interaction to achieve high-performance alkaline hydrogen evolution, Adv. Energy Mater. 12 (2022) 2200110.
[28] Y. Yao, Z. Huang, P. Xie, S.D. Lacey, R.J. Jacob, H. Xie, F. Chen, A. Nie, T. Pu, M. Rehwoldt, Carbothermal shock synthesis of high-entropy-alloy nanoparticles, Science 359 (2018) 1489.
[29] S. Dou, J. Xu, X. Cui, W. Liu, Z. Zhang, Y. Deng, W. Hu, Y. Chen, High-temperature shock enabled nanomanufacturing for energy-related applications, Adv. Energy Mater. 10 (2020) 2001331.
[30] S. Liu, Y. Shen, Y. Zhang, B. Cui, S. Xi, J. Zhang, L. Xu, S. Zhu, Y. Chen, Y. Deng, Extreme environmental thermal shock induced dislocation-rich Pt nanoparticles boosting hydrogen evolution reaction, Adv. Mater. 34 (2022) 2106973.
[31] Y. Liu, X. Tian, Y.-C. Han, Y. Chen, W. Hu, High-temperature shock synthesis of high-entropy-alloy nanoparticles for catalysis, Chin. J. Catal. 48 (2023) 66.
[32] Y. Chen, Y. Rao, R. Wang, Y. Yu, Q. Li, S. Bao, M. Xu, Q. Yue, Y. Zhang, Y. Kang, Interfacial engineering of Ni/V_2O_3 for hydrogen evolution reaction, Nano Res. 13 (2020) 2407.
[33] S. De, J. Zhang, R. Luque, N. Yan, Ni-based bimetallic heterogeneous catalysts for energy and environmental applications, Energy Environ. Sci. 9 (2016) 3314.
[34] J. Liu, Z. Wang, D. Zhang, Y. Qin, J. Xiong, J. Lai, L. Wang, Systematic engineering on Ni-based nanocatalysts effectively promote hydrogen evolution reaction, Small 18 (2022) 2108072.
[35] X. Bai, Q.-Q. Pang, X. Du, S.-S. Yi, S. Zhang, J. Qian, X.-Z. Yue, Z.-Y. Liu, Integrating RuNi alloy in S-doped defective carbon for efficient hydrogen evolution in both acidic and alkaline media, Chem. Eng. J. 417 (2021) 129319.
[36] J. Sun, P. Leng, Y. Xie, X. Yu, K. Qu, L. Feng, H. Bao, F. Luo, Z. Yang, Co single atoms and Co nanoparticle relay electrocatalyst for rechargeable zinc air batteries, Appl. Catal. B: Environ. 319 (2022) 121905.
[37] F. Chen, Y. Yao, A. Nie, S. Xu, J. Dai, E. Hitz, Y. Li, A. Lu, Z. Huang, T. Li, High-temperature atomic mixing toward well-dispersed bimetallic electrocatalysts, Adv. Energy Mater. 8 (2018) 1800466.
[38] Y. Chen, G.C. Egan, J. Wan, S. Zhu, R.J. Jacob, W. Zhou, J. Dai, Y. Wang, V.A. Danner, Y. Yao, Ultra-fast self-assembly and stabilization of reactive nanoparticles in reduced graphene oxide films, Nat. Commun. 7 (2016) 12332.
[39] J. Cheng, D. Wang, 2D materials modulating layered double hydroxides for electrocatalytic water splitting, Chin. J. Catal. 43 (2022) 1380.
[40] S. Banerjee, X. Han, V.S. Thoi, Modulating the electrode-electrolyte interface with cationic surfactants in carbon dioxide reduction, ACS Catal. 9 (2019) 5631.
[41] L. Wang, L. Duan, R.B. Ambre, Q. Daniel, H. Chen, J. Sun, B. Das, A. Thapper, J. Uhlig, P. Dinér, A nickel (II) PY5 complex as an electrocatalyst for water oxidation, J. Catal. 335 (2016) 72.
[42] M. Zhang, M.T. Zhang, C. Hou, Z.F. Ke, T.B. Lu, Homogeneous electrocatalytic water oxidation at neutral pH by a robust macrocyclic nickel (II) complex, Angew. Chem. Int. Ed. 126 (2014) 13258.
[43] Y.Y. Zhang, N. Zhang, P. Peng, R. Wang, Y. Jin, Y.K. Lv, X. Wang, W. Wei, S.Q. Zang, Uniformly dispersed Ru nanoparticles constructed by in situ confined polymerization of ionic liquids for the electrocatalytic hydrogen evolution reaction, Small Methods 5 (2021) 2100505.
[44] W. Feng, Y. Feng, J. Chen, H. Wang, Y. Hu, T. Luo, C. Yuan, L. Cao, L. Feng, J. Huang, Interfacial electronic engineering of Ru/FeRu nanoparticles as efficient trifunctional electrocatalyst for overall water splitting and Zn-air battery, Chem. Eng. J. 437 (2022) 135456.
[45] J. Gao, Y. Hu, Y. Wang, X. Lin, K. Hu, X. Lin, G. Xie, X. Liu, K.M. Reddy, Q. Yuan, MOF structure engineering to synthesize Co-N-C catalyst with richer accessible active sites for enhanced oxygen reduction, Small 17 (2021) 2104684.
[46] Z.-Y. Wu, P. Zhu, D.A. Cullen, Y. Hu, Q.-Q. Yan, S.-C. Shen, F.-Y. Chen, H. Yu, M. Shakouri, J.D. Arregui-Mena, A general synthesis of single atom catalysts with controllable atomic and mesoporous structures, Nat. Synth. 1 (2022) 658.
[47] S.H. Ahn, X. Yu, A. Manthiram, "Wiring" Fe-N_x-embedded porous carbon framework onto 1D nanotubes for efficient oxygen reduction reaction in alkaline and acidic media, Adv. Mater. 29 (2017) 1606534.
[48] J. Chen, J. Huang, Y. Zhao, L. Cao, K. Kajiyoshi, Y. Liu, Z. Li, Y. Feng, Enhancing the electronic metal-support interaction of CoRu alloy and pyridinic N for electrocatalytic pH-universal hydrogen evolution reaction, Chem. Eng. J. 450 (2022) 138026.
[49] Y. Liu, X. Li, Q. Zhang, W. Li, Y. Xie, H. Liu, L. Shang, Z. Liu, Z. Chen, L. Gu, A general route to prepare low-ruthenium-content bimetallic electrocatalysts for pH-universal hydrogen evolution reaction by using carbon quantum dots, Angew. Chem. Int. Ed. 59 (2020) 1718.
[50] G. Zhao, K. Rui, S.X. Dou, W. Sun, Heterostructures for electrochemical hydrogen evolution reaction: a review, Adv. Funct. Mater. 28 (2018) 1803291.
[51] W.-D. Zhang, Q.-T. Hu, L.-L. Wang, J. Gao, H.-Y. Zhu, X. Yan, Z.-G. Gu, In-situ generated Ni-MOF/LDH heterostructures with abundant phase interfaces for enhanced oxygen evolution reaction, Appl. Catal. B: Environ. 286 (2021) 119906.
[52] H. Yuan, F. Liu, G. Xue, H. Liu, Y. Wang, Y. Zhao, X. Liu, X. Zhang, L. Zhao, Z. Liu, Laser patterned and bifunctional Ni@N-doped carbon nanotubes as electrocatalyst and photothermal conversion layer for water splitting driven by thermoelectric device, Appl. Catal. B: Environ. 283 (2021) 119647.